Research Square

Preprints are preliminary reports that have not undergone peer review.
They should not be considered conclusive, used to inform clinical practice,
or referenced by the media as validated information.

A heterozygous nonsense variant in FGF8 causes autosomal dominant cleft lip and palate by impairing ERK–ETV4 signaling

Hao Shi
shihao198902080163.com
The First Affiliated Hospital of Zhengzhou University
Jingya Yang
The First Affiliated Hospital of Zhengzhou University
Yue Ma
The First Affiliated Hospital of Zhengzhou University
Chuanju Chen
The First Affiliated Hospital of Zhengzhou University
Wenbin Niu
The First Affiliated Hospital of Zhengzhou University
Ningzhao Ma
The First Affiliated Hospital of Zhengzhou University
Yidong Liu
The First Affiliated Hospital of Zhengzhou University
Haisong Wang
The First Affiliated Hospital of Zhengzhou University

Research Article

Keywords: cleft lip and palate, FGF8, nonsense variant, ERK signaling, ETV4, preimplantation genetic testing

Posted Date: May 20th, 2026

DOI: https://doi.org/10.21203/rs.3.rs-9623523/v1

License: This work is licensed under a Creative Commons Attribution 4.0 International License. Read Full License

Additional Declarations: No competing interests reported.

Abstract

Cleft lip and palate is a common craniofacial malformation, but the genetic basis of many familial cases remains unresolved. Here, we investigated a three-generation Chinese family with autosomal dominant cleft lip and palate and identified a heterozygous nonsense variant in *FGF8* (NM_033163.5:c.533G > A, p.(Trp178Ter); ClinVar accession SCV007520554). The variant was present in affected individuals and absent from unaffected family members, consistent with segregation with disease in the pedigree. Functional analyses in HEK-293T cells and primary mouse embryonic palatal mesenchymal cells showed that the truncated FGF8 protein was secreted but markedly reduced ERK1/2 phosphorylation and ETV4 expression. Expression of FGF8-ΔC impaired cell migration and proliferation, two cellular processes essential for palatal outgrowth and morphogenesis. Structural modeling suggested that the C-terminal truncation preserves the core FGF fold but disrupts key receptor-interacting contacts, supporting a plausible dominant-negative mechanism in which the mutant protein may occupy fibroblast growth factor receptors without efficiently activating downstream signaling. Preimplantation genetic testing for monogenic disease was subsequently performed, leading to the birth of a healthy infant who did not carry the familial variant. These findings expand the variant spectrum of FGF8-related craniofacial disorders and implicate impaired FGF8–ERK–ETV4 signaling in familial cleft lip and palate.

Introduction

Cleft lip and palate is among the most common congenital craniofacial anomalies, with an estimated incidence of approximately 1 in 500 to 1 in 2500 live births worldwide (Hammond and Dixon 2022; Mossey et al. 2009). The prevalence varies substantially across geographic regions and ethnic groups, with relatively high rates reported in Asian populations (Allori et al. 2017; Vyas et al. 2020). In addition to the visible craniofacial defect, cleft lip and palate can cause feeding difficulty, speech impairment, hearing problems and psychosocial morbidity. Its management often requires prolonged multidisciplinary care and imposes substantial medical and social burdens on affected individuals and families (Dixon et al. 2011; Mossey et al. 2009).

Normal development of the lip and palate depends on precisely coordinated morphogenetic processes, including neural crest cell contribution, cell migration, mesenchymal proliferation, palatal shelf growth, elevation, adhesion and fusion (Gritli-Linde 2007; Hammond and Dixon 2022; Ji et al. 2020). Neural crest-derived mesenchyme contributes substantially to early craniofacial morphogenesis, and disruption of proliferation or migration within craniofacial prominences can impair orofacial development and result in clefting phenotypes (Compagnucci et al. 2021; Gritli-Linde 2007; Ji et al. 2020).

Cleft lip and palate is etiologically heterogeneous. Approximately 70% of cases are non-syndromic and are thought to reflect complex interactions between genetic susceptibility and environmental exposures (Beaty et al. 2011; Dixon et al. 2011; Saleem et al. 2019). Reported environmental risk factors include maternal smoking, alcohol exposure, folate deficiency, ionizing radiation and viral infection (Babai and Irving 2023; DeRoo et al. 2008; Dixon et al. 2011). In contrast, syndromic and familial forms are more often caused by rare monogenic variants or chromosomal abnormalities (Babai and Irving 2023; Basha et al. 2018).

Fibroblast growth factor signaling is a major regulatory pathway controlling proliferation, migration, differentiation and survival during embryogenesis (Böttcher and Niehrs 2005; Brewer et al. 2016; Xie et al. 2020). Among FGF ligands, FGF8 is a key craniofacial morphogen involved in early facial patterning and outgrowth (Hao et al. 2019; Riley et al. 2007). Rare variants in FGF8 have been reported in developmental disorders, including hypogonadotropic hypogonadism and craniofacial anomalies, and impaired FGF signaling has been implicated in cleft lip and palate (Falardeau et al. 2008; Riley et al. 2007). However, the mechanisms by which FGF8 disruption contributes to human familial cleft lip and palate remain incompletely understood.

In this study, we investigated a three-generation Chinese family with autosomal dominant cleft lip and palate and identified a novel heterozygous nonsense variant in *FGF8*, NM_033163.5:c.533G > A, p.(Trp178Ter). We performed functional assays in HEK-293T cells and primary mouse embryonic palatal mesenchymal cells to assess the effect of the variant on FGF8 signaling and cell behavior. Our results indicate that the truncated FGF8 protein impairs ERK–ETV4 signaling and compromises cell migration and proliferation. Structural modeling further supports a plausible dominant-negative mechanism. Finally, we demonstrate the clinical utility of this genetic diagnosis through successful preimplantation genetic testing for monogenic disease.

Materials and methods

Study participants and ethical approval

This study was approved by the Ethics Committee of the First Affiliated Hospital of Zhengzhou University, Zhengzhou, China, approval number 2022-KY-1554. The study was conducted in accordance with the principles of the Declaration of Helsinki. Written informed consent was obtained from all participating family members or their legal guardians. Written informed consent for publication of clinical information, pedigree data, genetic findings and imaging data was also obtained.

A three-generation Han Chinese family with cleft lip and palate was recruited from the Center for Reproductive Medicine, The First Affiliated Hospital of Zhengzhou University. Clinical information was collected through detailed medical history, physical examination, prenatal ultrasound records and reproductive history.

Whole-exome sequencing and variant analysis

Genomic DNA was extracted from fetal tissue using the QIAamp DNA Mini Kit (Qiagen, Hilden, Germany) according to the manufacturer's protocol. Whole-exome sequencing was performed using the BGIV4 capture chip and MGISEQ-2000 platform. Sequencing reads were aligned to the human reference genome GRCh37/hg19 using BWA. Variants were called using GATK and annotated using ANNOVAR.

Candidate variants were filtered according to the following criteria: minor allele frequency ≤ 1% in population databases, including 1000 Genomes, ExAC, ESP6500 and gnomAD; predicted protein-altering effect; consistency with the inheritance pattern in the family; and biological relevance to craniofacial development based on OMIM and published literature. The transcript NM_033163.5 was used for *FGF8* variant annotation.

Sanger sequencing validation

PCR primers flanking the *FGF8* variant site were designed using Primer3. PCR amplification was performed using genomic DNA from available family members. PCR products were purified and subjected to Sanger sequencing. Sequence traces were analyzed to determine the presence or absence of the heterozygous *FGF8* NM_033163.5:c.533G > A variant.

Pathogenicity assessment

Variant pathogenicity was assessed according to the standards and guidelines of the American College of Medical Genetics and Genomics and the Association for Molecular Pathology (Richards et al. 2015). Evidence codes were assigned based on population frequency, predicted molecular consequence, segregation in the family, computational predictions and functional assay results. Bioinformatic predictions were performed using MutationTaster, PolyPhen-2 and PROVEAN. Cross-species conservation analysis was conducted using MEGA, with protein sequences retrieved from NCBI. The variant was submitted to ClinVar under accession number SCV007520554.

Cell culture and transfection

HEK-293T cells were obtained from Procell Life Science & Technology and cultured in Dulbecco's modified Eagle medium supplemented with 10% fetal bovine serum and 1% penicillin–streptomycin. HEK-293T cells were authenticated by short tandem repeat profiling and routinely tested to confirm absence of mycoplasma contamination.

Primary mouse embryonic palatal mesenchymal cells were isolated from E13.5 C57BL/6 embryos as previously described (Xiao et al. 2006). Briefly, palatal shelves were dissected and digested with Dispase II overnight at 4°C. The mesenchymal cells were separated from epithelial sheets and cultured in DMEM/F12 medium supplemented with 10% fetal bovine serum.

Human *FGF8* wild-type and mutant cDNA constructs were generated based on transcript NM_033163.5. Mouse *Fgf8* wild-type and mutant cDNA constructs were generated based on transcript NM_001379140. The mutant constructs carried the corresponding c.533G > A nonsense variant. Human constructs contained an N-terminal GFP tag. Cells were transfected using Lipofectamine 3000 according to the manufacturer's protocol and harvested 48 h after transfection.

Immunofluorescence staining

Primary mouse embryonic palatal mesenchymal cells were fixed with 4% paraformaldehyde, permeabilized with 0.5% Triton X-100 and blocked with goat serum. Cells were incubated with primary antibodies against vimentin or cytokeratin-19 overnight at 4°C. Cells were then incubated with Alexa Fluor 488-conjugated secondary antibody and counterstained with DAPI. Images were acquired using a fluorescence microscope.

Western blot analysis

Cells were lysed in RIPA buffer supplemented with PMSF and phosphatase inhibitors. Protein concentrations were determined using the BCA assay. Equal amounts of protein were separated by SDS–PAGE and transferred to nitrocellulose membranes. Membranes were blocked with 5% non-fat milk and incubated with primary antibodies against GFP-tag, FGF8, phospho-ERK1/2, total ERK1/2, ETV4/PEA3 or GAPDH overnight at

4°C. After incubation with HRP-conjugated secondary antibodies, signals were detected using enhanced chemiluminescence and quantified using ImageJ.

Enzyme-linked immunosorbent assay

FGF8 concentrations in cell culture supernatants were measured using Human FGF8 ELISA Kit (Cusabio) or Mouse FGF8 ELISA Kit (Lcsw Bio) according to the manufacturers' protocols.

Transwell migration assay

Transfected cells (8×10^4) were seeded in the upper chamber of Transwell inserts (Corning) with 2% FBS medium, while the lower chamber contained 10% FBS medium. After 24 h, cells that migrated through the membrane were fixed with methanol, stained with 0.1% crystal violet, and counted under a microscope in five random fields.

Cell proliferation assay

Transfected cells (4×10^3 per well) were seeded in 96-well plates. At indicated time points, CCK-8 reagent (Dojindo) was added and incubated for 1.5 h. Absorbance at 450 nm was measured using a microplate reader.

Transcriptomic data analysis of embryonic facial prominences

To evaluate the spatiotemporal expression patterns of *Fgf8* and *Etv4* during craniofacial development *in vivo*, public microarray dataset GSE7759 was downloaded from the NCBI Gene Expression Omnibus (GEO) database. This dataset contains transcriptomic profiles of distinct facial prominences (frontonasal, maxillary, and mandibular) isolated from wild-type mouse embryos at developmental stages E10.0 to E12.5. The normalized expression values (log2 RMA) of *Fgf8* and *Etv4* were extracted and visualized using R 4.5.2 to assess their co-expression dynamics during critical windows of palatogenesis.

Protein–protein interaction and structural modeling

The FGF8 protein–protein interaction network was analyzed using the STRING database. Direct and functionally associated interaction partners were identified with default confidence settings, and known interactions with FGFR1, FGFR2, FGFR3, FGFR4 and heparan sulfate-related components were inspected. Three-dimensional structures of wild-type FGF8, FGF8-ΔC and their predicted complexes with the FGFR2 extracellular domain were modeled using AlphaFold3. The wild-type human FGF8 sequence was derived from transcript NM_033163.5. The FGF8-ΔC sequence corresponded to the predicted product of NM_033163.5:c.533G > A, p.(Trp178Ter), retaining amino acids 1–177 and lacking the C-terminal 66 amino acids. Predicted models were visualized using PyMOL. Structural comparisons focused on preservation of the FGF core fold, loss of the C-terminal region and predicted differences in the ligand–receptor interface. Because these analyses were computational predictions, structural results were interpreted as supporting a plausible mechanistic model rather than providing direct biochemical evidence of receptor binding or activation.

Preimplantation genetic testing for monogenic disease

The affected female patient (II-2) underwent controlled ovarian hyperstimulation using a long GnRH agonist protocol. Mature oocytes were fertilized by intracytoplasmic sperm injection, and embryos were cultured to the blastocyst stage. Trophectoderm biopsy was performed, and biopsied cells were subjected to whole-genome amplification using the REPLI-g Single Cell Kit (Qiagen).

SNP microarray analysis was performed using HumanKaryomap-12 BeadChip (Illumina) and scanned on an iScan SQ system. Karyomapping analysis was conducted using BlueFuse Multi software to establish disease-linked haplotypes and determine embryo carrier status. Aneuploidy was assessed based on B-allele frequency and log R ratio plots.

Prenatal diagnosis

Amniocentesis was performed at 16–24 weeks of gestation. Fetal DNA was extracted and subjected to Sanger sequencing to verify the PGT-M result. Copy number variation sequencing (CNV-seq) was performed to assess chromosomal integrity. Prenatal ultrasound was used to evaluate fetal facial development.

Statistical analysis

All experiments were performed with at least three biological replicates. Data are presented as mean ± standard deviation. Statistical analyses were performed using GraphPad Prism 10. Comparisons between two groups were made using unpaired Student's t-test. CCK-8 data were analyzed using two-way ANOVA. A value of $P < 0.05$ was considered statistically significant. Significance levels are indicated as follows: * $P < 0.05$; ** $P < 0.01$; *** $P < 0.001$; **** $P < 0.0001$; ns, not significant.

Results

Identification of a novel FGF8 nonsense variant in a three-generation CLP family

We ascertained a three-generation Han Chinese family comprising seven members, of whom three were clinically affected with cleft lip and palate (Fig. 1a). The proband, individual II-2, was a female patient presenting with cleft lip and palate, dysarthria and choking during feeding. Her first pregnancy, individual III-1, was terminated after prenatal ultrasound detection of cleft lip and palate at 22 weeks of gestation. During her second pregnancy, ultrasound examination at 23 + 5 weeks revealed bilateral cleft lip and palate in fetus III-2, characterized by discontinuity of the upper lip and alveolar ridge, hypoplastic nasal alae and nasal collapse (Fig. 1b). The first-generation members, I-1 and I-2, and the proband's spouse, II-3, showed no craniofacial abnormalities.

To identify the genetic cause of disease in this family, whole-exome sequencing was performed using DNA extracted from fetal tissue of individual III-2. After filtering against population databases, including 1000 Genomes, ExAC, ESP6500 and gnomAD, and prioritizing rare coding variants in genes involved in craniofacial development, we identified a heterozygous nonsense variant in *FGF8*, NM_033163.5:c.533G > A, p.(Trp178Ter), as the most plausible candidate. Sanger sequencing confirmed the presence of this variant in the affected proband II-2 and the affected fetus III-2, whereas unaffected family members I-1, I-2 and II-3 carried only the reference allele (Fig. 1c). The variant was absent from major population databases and, to our knowledge, has not been reported previously in association with cleft lip and palate. The segregation pattern was consistent with autosomal dominant inheritance, with apparent de novo occurrence in the proband followed by vertical transmission to the affected fetus. The variant has been submitted to ClinVar under accession number SCV007520554.

According to ACMG/AMP guidelines, the variant was classified as likely pathogenic based on its predicted truncating effect in a disease-relevant gene, absence from population databases, segregation with disease in the family and functional evidence showing impaired FGF8 signaling. Specifically, PM2, PP1, PP3 and PS3_supporting/moderate were considered. PVS1 was considered with caution and at reduced strength because the variant is predicted to produce a truncated protein rather than necessarily undergo complete nonsense-mediated decay, and our functional data support a dominant-negative effect rather than simple haploinsufficiency. Multiple bioinformatic tools, including MutationTaster, PolyPhen-2 and PROVEAN, consistently predicted the variant to be deleterious. Cross-species alignment showed that the tryptophan residue at position 178 is highly conserved across vertebrates, including human, chimpanzee, rhesus macaque, mouse and zebrafish (Fig. 1d). Schematic protein analysis indicated that p.(Trp178Ter) generates a truncated protein of 177 amino acids lacking the final 66 amino acids of the FGF8 C terminus (Fig. 1e).

FGF8-ΔC impairs ERK–ETV4 signaling in HEK-293T cells

To investigate the functional consequences of the FGF8 variant, we constructed expression vectors encoding GFP-tagged wild-type human FGF8 and the C-terminally truncated mutant protein, hereafter referred to as FGF8 and FGF8-ΔC, respectively. These constructs were transfected into HEK-293T cells. Western blot analysis showed that GFP-FGF8-ΔC migrated at approximately 48 kDa, compared with approximately 54 kDa for GFP-tagged wild-type FGF8, confirming production of a truncated protein (Fig. 2a).

The ERK1/2 pathway is a well-established downstream effector of FGF signaling and regulates cell migration and proliferation during embryonic development (Brewer et al. 2016; Xie et al. 2020). ETV4, also known as PEA3, is a member of the PEA3 subfamily of ETS transcription factors. Previous studies have shown that PEA3/ETV4 activity is closely coupled to ERK MAP kinase signaling, and Fgf-dependent Etv4/5 activity is required for developmental patterning in embryonic tissues (Mao et al. 2009; Keld et al. 2010; Oh et al. 2012). We therefore examined whether FGF8-ΔC affects this signaling axis. Western blot analysis revealed that ERK1/2 phosphorylation was significantly reduced in FGF8-ΔC-transfected cells compared with wild-type FGF8-transfected cells ($P < 0.001$; Fig. 2b,c). Correspondingly, ETV4 protein expression was markedly decreased in FGF8-ΔC-transfected cells ($P < 0.0001$; Fig. 2b,c). In this overexpression system, wild-type FGF8 did not significantly increase p-ERK1/2 or ETV4 levels relative to baseline, whereas FGF8-ΔC reduced both signaling readouts. These findings suggest that FGF8-ΔC does not act solely through reduced ligand dosage but exerts an inhibitory effect on ERK–ETV4 signaling.

Because FGF8 functions as a secreted paracrine signaling molecule, we examined whether the truncating variant affected FGF8 secretion. ELISA quantification of FGF8 in cell culture supernatants showed no significant difference between wild-type FGF8- and FGF8-ΔC-transfected cells ($P = 0.6941$; Fig. 2d), suggesting that loss of the C-terminal region does not substantially impair secretion in this system.

To evaluate the developmental relevance of the FGF8–ETV4 signaling axis in vivo, we analyzed the public craniofacial transcriptomic dataset GSE7759, which profiles gene expression in mouse facial prominences from E10.0 to E12.5 (Feng et al. 2009). Expression profiling of the frontonasal, mandibular and maxillary prominences, the primary embryonic structures contributing to lip and palate formation, showed that both genes are expressed during the critical morphogenetic window from embryonic day 10.0 to 12.5 (Fig. 2e). The expression trajectory of *Etv4* closely paralleled or followed robust early expression of *Fgf8* across these facial prominences. This in vivo co-expression pattern supports *ETV4* as a physiological downstream effector of *FGF8* signaling during craniofacial morphogenesis.

FGF8-ΔC inhibits HEK-293T cell migration and proliferation

Because cell migration and proliferation are essential for craniofacial morphogenesis and palatal development, we next assessed the effect of FGF8-ΔC on these cellular processes. Transwell migration assays showed that HEK-293T cells transfected with FGF8-ΔC exhibited significantly reduced migratory capacity compared with cells transfected with wild-type FGF8 ($P < 0.001$; Fig. 3a,b). CCK-8 proliferation assays further showed that FGF8-ΔC significantly impaired cell proliferation over a 4-day time course compared with wild-type FGF8 ($P < 0.01$ to $P < 0.0001$ at different time points; Fig. 3c). These results indicate that the p.(Trp178Ter) variant compromises cellular behaviors regulated by FGF8 signaling.

FGF8-ΔC impairs ERK–ETV4 signaling, migration and proliferation in primary mouse embryonic palatal mesenchymal cells

To validate the functional findings in a more developmentally relevant cellular model, we isolated primary mouse embryonic palatal mesenchymal cells from E13.5 C57BL/6 embryos. Immunofluorescence staining confirmed the mesenchymal identity of these cells, as shown by positive vimentin staining and absence of cytokeratin-19 staining (Fig. 4a,b).

We next constructed mouse Fgf8 wild-type and mutant expression vectors and transfected them into primary mouse embryonic palatal mesenchymal cells. Western blot analysis confirmed altered protein detection in mutant-transfected cells. The mutant protein was not detected by the FGF8 antibody because of loss of the antibody epitope region, whereas a faint band in the mutant lane likely represented endogenous FGF8 (Fig. 4c). Importantly, Fgf8-ΔC significantly reduced ERK1/2 phosphorylation ($P < 0.01$) and ETV4 protein expression ($P < 0.001$) in palatal mesenchymal cells compared with wild-type Fgf8 (Fig. 4d,e). ELISA analysis showed no significant difference in secreted FGF8 levels between groups ($P = 0.4838$; Fig. 4f), indicating that the mutant protein retained secretory capacity in these primary cells.

Functional assays further demonstrated that Fgf8-ΔC impaired cellular processes relevant to palatogenesis. To define the basal cellular state, we included an untransfected blank control group. In Transwell migration assays, wild-type Fgf8 promoted migration of palatal mesenchymal cells, whereas Fgf8-ΔC markedly reduced migration compared with the wild-type group and also suppressed migration below the level of the blank control ($P < 0.001$; Fig. 4g,h). This sub-baseline suppression is consistent with an inhibitory or dominant-negative effect, potentially through interference with endogenous FGF-dependent migratory signaling. In CCK-8 proliferation assays, Fgf8-ΔC-transfected cells showed greater proliferation than blank control cells but significantly less proliferation than wild-type Fgf8-transfected cells ($P < 0.01$ to $P < 0.0001$; Fig. 4i). Together with the observations in HEK-293T cells, these findings indicate that the C-terminally truncated FGF8 protein compromises ERK–ETV4 signaling and impairs migration and proliferation in palatal mesenchymal cells.

Structural modeling supports a plausible dominant-negative mechanism of FGF8-ΔC

To explore how the p.(Trp178Ter) variant might inhibit FGF8 signaling, we first analyzed the protein–protein interaction network of FGF8 using the STRING database. The network confirmed that fibroblast growth factor receptors FGFR1–FGFR4 are primary direct interaction partners of FGF8, with heparan sulfate proteoglycans also implicated in FGF signaling complex formation (Fig. 5a).

We next modeled the three-dimensional structures of wild-type FGF8, FGF8-ΔC and their predicted complexes with the FGFR2 extracellular domain using AlphaFold3. The predicted monomeric structure of wild-type FGF8 showed the characteristic FGF core fold, with the C-terminal region extending beyond the core domain (Fig. 5b). The FGF8-ΔC model indicated that the p.(Trp178Ter) variant removes the C-terminal 66 amino acids but largely preserves the core β-trefoil fold of the FGF homology domain (Fig. 5c,d).

Docking models of wild-type FGF8 and FGF8-ΔC with FGFR2 suggested a plausible structural basis for impaired receptor activation. In the predicted wild-type FGF8–FGFR2 complex, the C-terminal region of FGF8 extends into the receptor-binding groove and forms a network of polar contacts and hydrogen bonds that may stabilize the ligand–receptor interface (Fig. 5e). In contrast, the FGF8-ΔC model suggested that the preserved FGF core may retain the capacity to dock into the FGFR2 binding region, but absence of the C-terminal tail leaves a structural void at the interaction interface and eliminates several predicted stabilizing contacts (Fig. 5f). These observations support a dominant-negative model in which FGF8-ΔC may compete with endogenous ligand for receptor engagement while failing to induce efficient receptor activation and downstream ERK–ETV4 signaling.

Preimplantation genetic testing prevented transmission of the familial FGF8 variant

Based on the genetic and functional evidence, the affected couple received genetic counseling and underwent preimplantation genetic testing for monogenic disease, combined with aneuploidy screening. Following controlled ovarian stimulation and intracytoplasmic sperm injection, six blastocysts were obtained, and trophectoderm biopsy was performed.

Karyomapping is a genome-wide linkage-based approach for parental haplotype tracking in preimplantation genetic testing of monogenic disorders (Handyside et al. 2010; Fesahat et al. 2020; Madero et al. 2023). Using SNP microarray data from the couple, the affected fetus and the embryos, we defined disease-associated and wild-type maternal haplotypes across a 2-Mb interval flanking *FGF8*. Embryos 1, 2, 3 and 4 inherited the maternal wild-type haplotype, whereas embryos 5 and 6 inherited the disease-associated maternal haplotype carrying the *FGF8* variant

(Fig. 6a). Concurrent aneuploidy screening showed that embryo 3 carried trisomy 18 and was therefore not suitable for transfer. Embryos 1, 2 and 4 were euploid and did not carry the familial variant (Table 2; Fig. 6b).

Table 1
FGF8 mutation information and database results

Gene	Chromosome	Position	Nucleotide change	Amino acid change	Zygosity	Variant type	ESP6500	1000G	ExAC	gnomAD
FGF8	chr10	103530288	c.533G > A	p.(Trp178Ter)	Heterozygous	Nonsense	NA	NA	NA	NA

Table 2
Preimplantation genetic testing results for the family

Embryo	Karyotype	Variant status	Transferable
1	46,XN	Non-carrier	Yes
2	46,XN	Non-carrier	Yes
3	47,XN,+18	Non-carrier	No (aneuploidy)
4	46,XN	Non-carrier	Yes
5	46,XN	Carrier	No
6	46,XN	Carrier	No

One euploid embryo without the familial *FGF8* variant was transferred to the patient's uterus. Clinical pregnancy was confirmed 35 days after embryo transfer. Amniocentesis at mid-gestation confirmed that the fetus did not carry the *FGF8* NM_033163.5:c.533G > A, p.(Trp178Ter) variant (Fig. 6c). Prenatal ultrasound showed normal facial development without evidence of cleft lip or palate (Fig. 6d). The patient subsequently delivered a healthy infant without cleft lip or palate, demonstrating successful prevention of vertical transmission of the familial variant.

Discussion

In this study, we identified a novel heterozygous nonsense variant in *FGF8*, NM_033163.5:c.533G > A, p.(Trp178Ter), in a three-generation family with autosomal dominant cleft lip and palate. The variant was present in affected individuals and absent from unaffected family members tested in the pedigree, supporting segregation with disease. Functional analyses in HEK-293T cells and primary mouse embryonic palatal mesenchymal cells demonstrated that the truncated FGF8 protein impaired ERK1/2 phosphorylation, reduced ETV4 expression, and compromised cell migration and proliferation. Structural modeling further supported a plausible dominant-negative mechanism. Finally, preimplantation genetic testing for monogenic disease was successfully used to prevent transmission of the familial variant.

Our findings expand the mutational and mechanistic spectrum of FGF8-related craniofacial disease. FGF signaling is essential for craniofacial morphogenesis, and perturbation of this pathway has been linked to cleft lip and palate in humans and animal models (Brewer et al. 2016; Riley et al. 2007; Xie et al. 2020). FGF8 is particularly important during early facial patterning and outgrowth, functioning as a secreted morphogen that coordinates epithelial–mesenchymal signaling, proliferation and regional identity (Böttcher and Niehrs 2005; Hao et al. 2019). Previous studies have implicated rare *FGF8* variants in developmental disorders, including hypogonadotropic hypogonadism and craniofacial phenotypes (Falardeau et al. 2008; Riley et al. 2007). However, direct functional evidence linking a familial *FGF8* truncating variant to impaired palatal mesenchymal cell behavior has remained limited. The present study provides genetic, cellular and structural evidence supporting the pathogenic relevance of a novel *FGF8* nonsense variant in familial cleft lip and palate.

The functional data favor an inhibitory or dominant-negative mechanism rather than simple haploinsufficiency alone. The mutant protein was secreted at levels comparable to wild-type FGF8 in both HEK-293T cells and primary palatal mesenchymal cells. Nevertheless, FGF8-ΔC reduced ERK1/2 phosphorylation and ETV4 expression, indicating impaired downstream signaling. In primary mouse embryonic palatal mesenchymal cells, Fgf8-ΔC suppressed migration not only relative to wild-type Fgf8 but also below the basal level observed in blank control cells. This sub-baseline effect suggests that the truncated protein may interfere with endogenous FGF-dependent migratory cues. Such an effect would be difficult to explain by reduced gene dosage alone and is more consistent with a mutant ligand that competes for receptor engagement but fails to activate productive signaling.

This interpretation is supported by structural modeling. The predicted FGF8-ΔC protein retains the core β-trefoil fold but lacks the C-terminal 66 amino acids. In the predicted wild-type FGF8–FGFR2 complex, this C-terminal region contributes multiple stabilizing contacts at the ligand–receptor interface. Loss of this region in FGF8-ΔC leaves a structural void and eliminates predicted receptor-interacting contacts. These findings are compatible with a model in which FGF8-ΔC can partially dock into the receptor-binding region through the preserved core domain but cannot efficiently stabilize the FGF–FGFR signaling complex or promote receptor activation. Because FGF signaling requires ligand-induced receptor

dimerization and heparan sulfate-dependent stabilization of the signaling complex (Olsen et al. 2006; Schlessinger et al. 2000; Zhang et al. 2006), disruption of C-terminal ligand–receptor interactions could markedly reduce downstream ERK activation.

Nevertheless, structural modeling alone cannot prove receptor binding or dominant-negative activity. Direct biochemical measurements, such as surface plasmon resonance or isothermal titration calorimetry, will be required to compare the binding kinetics of wild-type FGF8 and FGF8-ΔC to FGFR1c and FGFR2c, two receptor isoforms relevant to craniofacial development. In addition, receptor phosphorylation assays and ligand competition experiments with varying ratios of wild-type and mutant FGF8 would provide more direct evidence for the proposed dominant-negative mechanism.

ETV4 emerged from our data as a candidate downstream mediator of FGF8 signaling in palatal mesenchymal cells. ETV4 belongs to the PEA3 subfamily of ETS transcription factors and is closely linked to RAS–ERK signaling (Keld et al. 2010; Oh et al. 2012). Our analysis of the GSE7759 dataset showed that *Fgf8* and *Etv4* are co-expressed in the frontonasal, mandibular and maxillary prominences during the critical developmental window from E10.0 to E12.5. These structures contribute to formation of the lip and palate, and their coordinated growth and morphogenesis require tightly regulated cell proliferation and migration (Gritli-Linde 2007; Hammond and Dixon 2022). The reduction of ETV4 expression after FGF8-ΔC expression in both HEK-293T and palatal mesenchymal cells therefore supports the relevance of the FGF8–ERK–ETV4 axis in craniofacial development.

Whether ETV4 is a required functional effector of FGF8 during palatogenesis remains to be determined. If ETV4 is necessary for FGF8-dependent migration and proliferation, forced ETV4 expression may rescue the cellular defects caused by FGF8-ΔC. Conversely, if ETV4 mainly serves as a readout of attenuated ERK signaling, activation of upstream ERK signaling, for example through constitutively active MEK, may restore cell behavior independently of ETV4. Future rescue experiments will be important for distinguishing these possibilities and for clarifying the position of ETV4 within the pathogenic pathway.

The use of primary mouse embryonic palatal mesenchymal cells strengthens the developmental relevance of our functional observations. Palatal mesenchymal proliferation drives palatal shelf outgrowth, whereas directional migration contributes to shelf elevation and midline convergence (Gritli-Linde 2007; Iwata et al. 2012). Impairment of either process can compromise palatal morphogenesis. In our study, Fgf8-ΔC reduced both migration and proliferation relative to wild-type Fgf8, suggesting that the variant affects multiple cellular behaviors required for normal palate development. The stronger suppression of migration below basal levels suggests that cell motility may be particularly sensitive to inhibitory FGF8 signaling in palatal mesenchymal cells. However, the relative contribution of defective migration versus defective proliferation to the clefting phenotype cannot be determined from cell culture experiments alone.

The preimplantation genetic testing results illustrate the clinical utility of identifying the causal variant in familial cleft lip and palate. The proband had experienced two previous pregnancies affected by cleft lip and palate, including prenatal diagnosis and pregnancy termination. Once the familial *FGF8* variant was identified and functionally supported, karyomapping-based preimplantation genetic testing enabled selection of embryos that did not inherit the maternal disease-associated haplotype. Combining monogenic testing with aneuploidy screening was clinically important, because one non-carrier embryo carried trisomy 18 and was therefore not suitable for transfer. Subsequent prenatal diagnosis confirmed the absence of the familial variant, and the birth of an unaffected infant demonstrated successful prevention of vertical transmission.

This study has several limitations. First, although the family structure supports autosomal dominant inheritance, the number of affected individuals is limited, and additional unrelated families or sporadic cases carrying deleterious *FGF8* variants would strengthen genotype–phenotype correlations. Second, the apparent de novo occurrence of the variant in the proband was inferred from Sanger sequencing of available parental samples; low-level parental mosaicism cannot be completely excluded without deep sequencing. Third, the proposed dominant-negative mechanism is supported by cellular assays and structural modeling but has not yet been confirmed by direct receptor-binding or receptor-activation assays. Fourth, although primary palatal mesenchymal cells provide a relevant developmental model, in vivo validation in an animal model is still lacking. A knock-in mouse model carrying the orthologous p.(Trp178Ter) variant would be particularly useful for assessing penetrance, expressivity, tissue-specific signaling defects and possible genetic modifiers.

In conclusion, we report a novel heterozygous *FGF8* nonsense variant associated with autosomal dominant cleft lip and palate and provide functional evidence that the truncated FGF8 protein impairs ERK–ETV4 signaling and palatal mesenchymal cell behavior. These findings expand the genetic spectrum of FGF8-related craniofacial disorders and support impaired FGF8–ERK–ETV4 signaling as a pathogenic mechanism in familial cleft lip and palate. The successful application of preimplantation genetic testing further highlights the clinical relevance of molecular diagnosis for hereditary craniofacial malformations.

Conclusion

In conclusion, we identified a novel heterozygous nonsense variant in FGF8, NM_033163.5:c.533G > A, p.(Trp178Ter), in a family with autosomal dominant cleft lip and palate. Genetic segregation, functional assays and structural modeling support the pathogenic relevance of this variant. The truncated FGF8 protein impaired ERK–ETV4 signaling and compromised migration and proliferation of palatal mesenchymal cells,

supporting impaired FGF8–ERK–ETV4 signaling as a mechanism underlying familial cleft lip and palate. The successful application of preimplantation genetic testing further highlights the clinical value of molecular diagnosis for hereditary craniofacial malformations.

Declarations

Acknowledgements

We thank the family members for their participation in this study.Statements and Declarations.

Author contributions

H.S. and H.W. conceived and designed the study. H.S., J.Y. and Y.M. performed the experiments, analyzed the data and drafted the manuscript. C.C., W.N. and N.M. collected clinical samples, interpreted clinical data and performed preimplantation genetic testing analysis. Y.L. performed bioinformatic analysis and structural modeling. H.S. and H.W. supervised the study, revised the manuscript and obtained funding. All authors critically reviewed the manuscript and approved the final version.

Funding

This work was supported by the Natural Science Foundation Project of Henan Province, China, grant number 242300421483 to Hao Shi.

Data availability

Because this study includes family-based human genetic data with potential re-identification risk, raw sequencing data are not publicly deposited. De-identified data supporting the findings of this study are available from the corresponding author upon reasonable request, subject to institutional review, ethics approval and applicable data access agreements. The public transcriptomic dataset analyzed in this study is available from the NCBI Gene Expression Omnibus under accession number GSE7759. The FGF8 variant NM_033163.5:c.533G>A, p.(Trp178Ter) has been submitted to ClinVar under accession number SCV007520554.

Conflict of interest

The authors declare that they have no competing interests.

Ethical approval and consent to participate

This study was approved by the Ethics Committee of the First Affiliated Hospital of Zhengzhou University, Zhengzhou, China, approval number 2022-KY-1554. The study was conducted in accordance with the principles of the Declaration of Helsinki. Written informed consent was obtained from all participating family members or their legal guardians.

Consent for publication

Written informed consent for publication of clinical information, pedigree data, genetic findings, ultrasound images and other potentially identifiable data was obtained from all participating individuals or their legal guardians.

References

1. Allori AC, Mulliken JB, Meara JG, Shusterman S, Marcus JR (2017) Classification of cleft lip/palate: then and now. Cleft Palate Craniofac J 54:175–188. https://doi.org/10.1597/14-080
2. Babai A, Irving M (2023) Orofacial clefts: genetics of cleft lip and palate. Genes 14:1603. https://doi.org/10.3390/genes14081603
3. Basha M, Demeer B, Revencu N, Helaers R, Theys S, Bou Saba S, Boute O, Devauchelle B, François G, Bayet B, Vikkula M (2018) Whole exome sequencing identifies mutations in 10% of patients with familial non-syndromic cleft lip and/or palate in genes mutated in well-known syndromes. J Med Genet 55:449–458. https://doi.org/10.1136/jmedgenet-2017-105110
4. Beaty TH, Ruczinski I, Murray JC, Marazita ML, Munger RG, Hetmanski JB, Murray T, Redett RJ, Fallin MD, Liang KY et al (2011) Evidence for gene-environment interaction in a genome wide study of nonsyndromic cleft palate. Genet Epidemiol 35:469–478. https://doi.org/10.1002/gepi.20595
5. Böttcher RT, Niehrs C (2005) Fibroblast growth factor signaling during early vertebrate development. Endocr Rev 26:63–77. https://doi.org/10.1210/er.2003-0040
6. Brewer JR, Mazot P, Soriano P (2016) Genetic insights into the mechanisms of Fgf signaling. Genes Dev 30:751–771. https://doi.org/10.1101/gad.277137.115

7. Compagnucci C, Martinus K, Griffin J, Depew MJ (2021) Programmed cell death not as sledgehammer but as chisel: apoptosis in normal and abnormal craniofacial patterning and development. Front Cell Dev Biol 9:717404. https://doi.org/10.3389/fcell.2021.717404
8. DeRoo LA, Wilcox AJ, Drevon CA, Lie RT (2008) First-trimester maternal alcohol consumption and the risk of infant oral clefts in Norway: a population-based case-control study. Am J Epidemiol 168:638–646. https://doi.org/10.1093/aje/kwn186
9. Dixon MJ, Marazita ML, Beaty TH, Murray JC (2011) Cleft lip and palate: understanding genetic and environmental influences. Nat Rev Genet 12:167–178. https://doi.org/10.1038/nrg2933
10. Falardeau J, Chung WCJ, Beenken A, Raivio T, Plummer L, Sidis Y, Jacobson-Dickman EE, Eliseenkova AV, Ma J, Dwyer A et al (2008) Decreased FGF8 signaling causes deficiency of gonadotropin-releasing hormone in humans and mice. J Clin Invest 118:2822–2831. https://doi.org/10.1172/JCI34538
11. Feng W, Leach SM, Tipney H, Phang T, Geraci M, Spritz RA, Hunter LE, Williams T (2009) Spatial and temporal analysis of gene expression during growth and fusion of the mouse facial prominences. PLoS ONE 4:e8066. https://doi.org/10.1371/journal.pone.0008066
12. Fesahat F, Montazeri F, Hoseini SM (2020) Preimplantation genetic testing in assisted reproduction technology. J Gynecol Obstet Hum Reprod 49:101723. https://doi.org/10.1016/j.jogoh.2020.101723
13. Gritli-Linde A (2007) Molecular control of secondary palate development. Dev Biol 301:309–326. https://doi.org/10.1016/j.ydbio.2006.07.042
14. Hammond NL, Dixon MJ (2022) Revisiting the embryogenesis of lip and palate development. Oral Dis 28:1306–1326. https://doi.org/10.1111/odi.14174
15. Handyside AH, Harton GL, Mariani B, Thornhill AR, Affara NA, Shaw MA, Griffin DK (2010) Karyomapping: a universal method for genome wide analysis of genetic disease based on mapping crossovers between parental haplotypes. J Med Genet 47:651–658. https://doi.org/10.1136/jmg.2009.069971
16. Hao Y, Tang S, Yuan Y, Liu R, Chen Q (2019) Roles of FGF8 subfamily in embryogenesis and oral-maxillofacial diseases. Int J Oncol 54:797–806. https://doi.org/10.3892/ijo.2019.4677
17. Iwata J, Tung L, Urata M, Hacia JG, Pelikan R, Suzuki A, Ramenzoni L, Chaudhry O, Parada C, Sanchez-Lara PA, Chai Y (2012) Fibroblast growth factor 9-pituitary homeobox 2 pathway mediates transforming growth factor β signaling to regulate cell proliferation in palatal mesenchyme during mouse palatogenesis. J Biol Chem 287:2353–2363. https://doi.org/10.1074/jbc.M111.280974
18. Ji Y, Garland MA, Sun B, Zhang S, Reynolds K, McMahon M, Schmidt C, Cheng L, Zhou CJ (2020) Cellular and developmental basis of orofacial clefts. Birth Defects Res 112:1558–1587. https://doi.org/10.1002/bdr2.1785
19. Keld R, Guo B, Downey P, Gulmann C, Ang YS, Sharrocks AD (2010) The ERK MAP kinase-PEA3/ETV4-MMP-1 axis is operative in oesophageal adenocarcinoma. Mol Cancer 9:313. https://doi.org/10.1186/1476-4598-9-313
20. Madero JI, Manotas MC, García-Acero M, López Cáceres A, López Jaimes C (2023) Preimplantation genetic testing in assisted reproduction. Minerva Obstet Gynecol 75:260–272. https://doi.org/10.23736/S2724-606X.21.04805-3
21. Mao J, McGlinn E, Huang P, Tabin CJ, McMahon AP (2009) Fgf-dependent Etv4/5 activity is required for posterior restriction of Sonic hedgehog and promoting outgrowth of the vertebrate limb. Dev Cell 16:600–606. https://doi.org/10.1016/j.devcel.2009.02.005
22. Mossey PA, Little J, Munger RG, Dixon MJ, Shaw WC (2009) Cleft lip and palate. Lancet 374:1773–1785. https://doi.org/10.1016/S0140-6736(09)60695-4
23. Oh S, Shin S, Janknecht R (2012) ETV1, 4 and 5: an oncogenic subfamily of ETS transcription factors. Biochim Biophys Acta 1826:1–12. https://doi.org/10.1016/j.bbcan.2012.02.002
24. Olsen SK, Li JYH, Bromleigh C, Eliseenkova AV, Ibrahimi OA, Lao Z, Zhang F, Linhardt RJ, Joyner AL, Mohammadi M (2006) Structural basis by which alternative splicing modulates the organizer activity of FGF8 in the brain. Genes Dev 20:185–198. https://doi.org/10.1101/gad.1365406
25. Richards S, Aziz N, Bale S, Bick D, Das S, Gastier-Foster J, Grody WW, Hegde M, Lyon E, Spector E et al (2015) Standards and guidelines for the interpretation of sequence variants: a joint consensus recommendation of the American College of Medical Genetics and Genomics and Association for Molecular Pathology. Genet Med 17:405–424. https://doi.org/10.1038/gim.2015.30
26. Riley BM, Mansilla MA, Ma J, Daack-Hirsch S, Maher BS, Raffensperger LM, Russo ET, Vieira AR, Dodé C, Mohammadi M, Marazita ML, Murray JC (2007) Impaired FGF signaling contributes to cleft lip and palate. Proc Natl Acad Sci USA 104:4512–4517. https://doi.org/10.1073/pnas.0607956104
27. Saleem K, Zaib T, Sun W, Fu S (2019) Assessment of candidate genes and genetic heterogeneity in human non-syndromic orofacial clefts specifically non-syndromic cleft lip with or without palate. Heliyon 5:e03019. https://doi.org/10.1016/j.heliyon.2019.e03019
28. Schlessinger J, Plotnikov AN, Ibrahimi OA, Eliseenkova AV, Yeh BK, Yayon A, Linhardt RJ, Mohammadi M (2000) Crystal structure of a ternary FGF-FGFR-heparin complex reveals a dual role for heparin in FGFR binding and dimerization. Mol Cell 6:743–750. https://doi.org/10.1016/S1097-2765(00)00073-3

29. Vyas T, Gupta P, Kumar S, Gupta R, Gupta T, Singh HP (2020) Cleft of lip and palate: a review. J Family Med Prim Care 9:2621–2625. https://doi.org/10.4103/jfmpc.jfmpc_472_20
30. Xiao WL, Shi B, Zheng Q, Wang Y, Huang L, Li S, Lu Y, Wu M (2007) Nucleofection is highly efficient for transfecting genes into murine embryonic palatal mesenchymal cells in primary culture. Int J Oral Maxillofac Surg 36:429–434. https://doi.org/10.1016/j.ijom.2006.12.008
31. Xie Y, Su N, Yang J, Tan Q, Huang S, Jin M, Ni Z, Zhang B, Zhang D, Luo F et al (2020) FGF/FGFR signaling in health and disease. Signal Transduct Target Ther 5:181. https://doi.org/10.1038/s41392-020-00222-7
32. Zhang X, Ibrahimi OA, Olsen SK, Umemori H, Mohammadi M, Ornitz DM (2006) Receptor specificity of the fibroblast growth factor family: the complete mammalian FGF family. J Biol Chem 281:15694–15700. https://doi.org/10.1074/jbc.M601252200

Figures

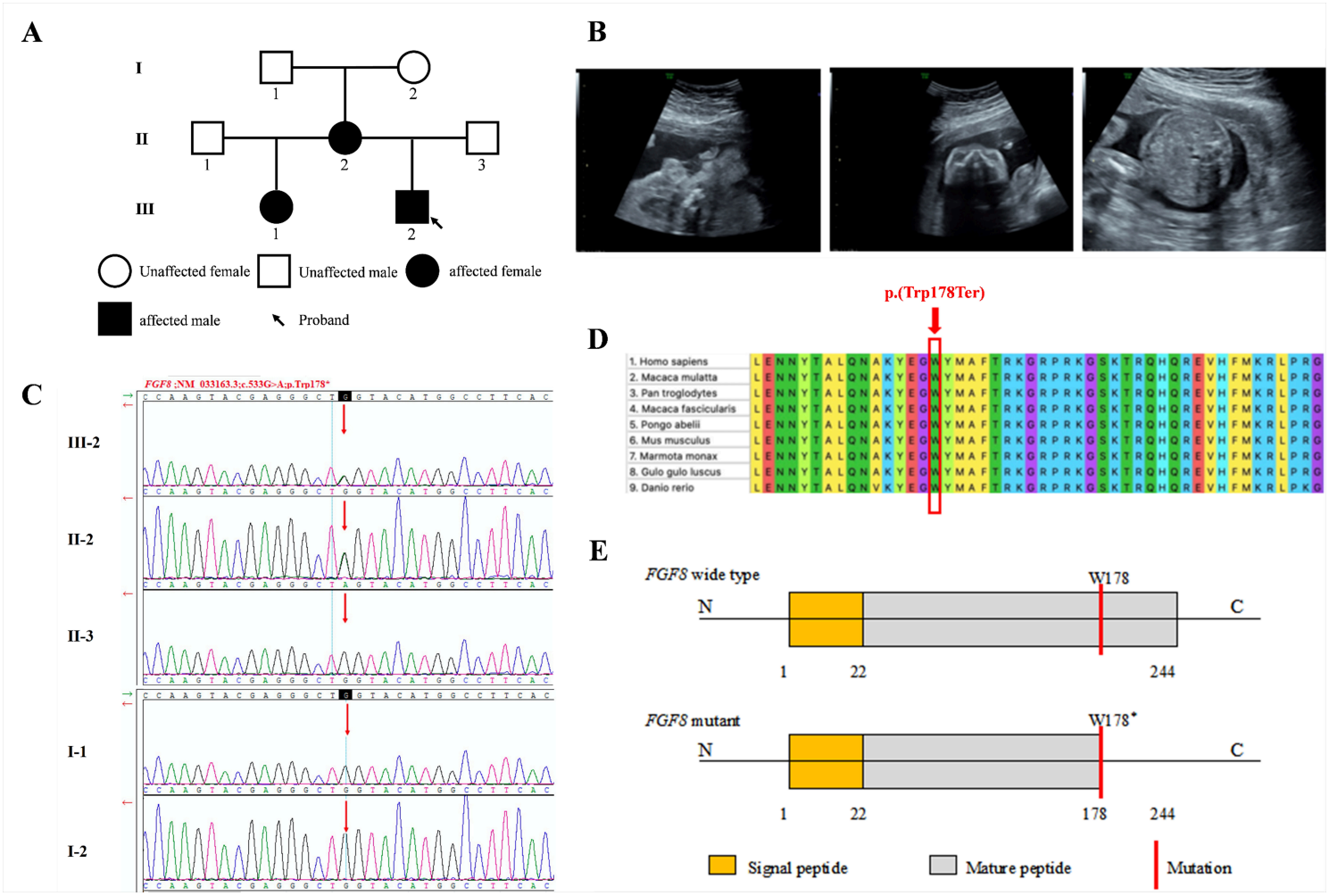


Figure 1

Identification of a heterozygous FGF8 nonsense variant in a family with cleft lip and palate.

A Pedigree of the three-generation family with cleft lip and palate. Filled symbols indicate affected individuals, open symbols indicate unaffected individuals, and the arrow indicates the proband. The *FGF8* NM_033163.5:c.533G>A, p.(Trp178Ter) variant segregated with the affected phenotype in available family members. B Prenatal ultrasound images of affected fetus III-2 showing bilateral cleft lip and palate, with discontinuity of the upper lip and alveolar ridge, hypoplastic nasal alae and nasal collapse. C Sanger sequencing chromatograms confirming the heterozygous c.533G>A variant in affected individuals II-2 and III-2 and the reference allele in unaffected family members I-1, I-2 and II-3. D Cross-species conservation analysis showing that Trp178 of FGF8 is highly conserved among vertebrates. E Schematic representation of the wild-type FGF8 protein and the predicted C-terminally truncated FGF8 protein generated by p.(Trp178Ter).

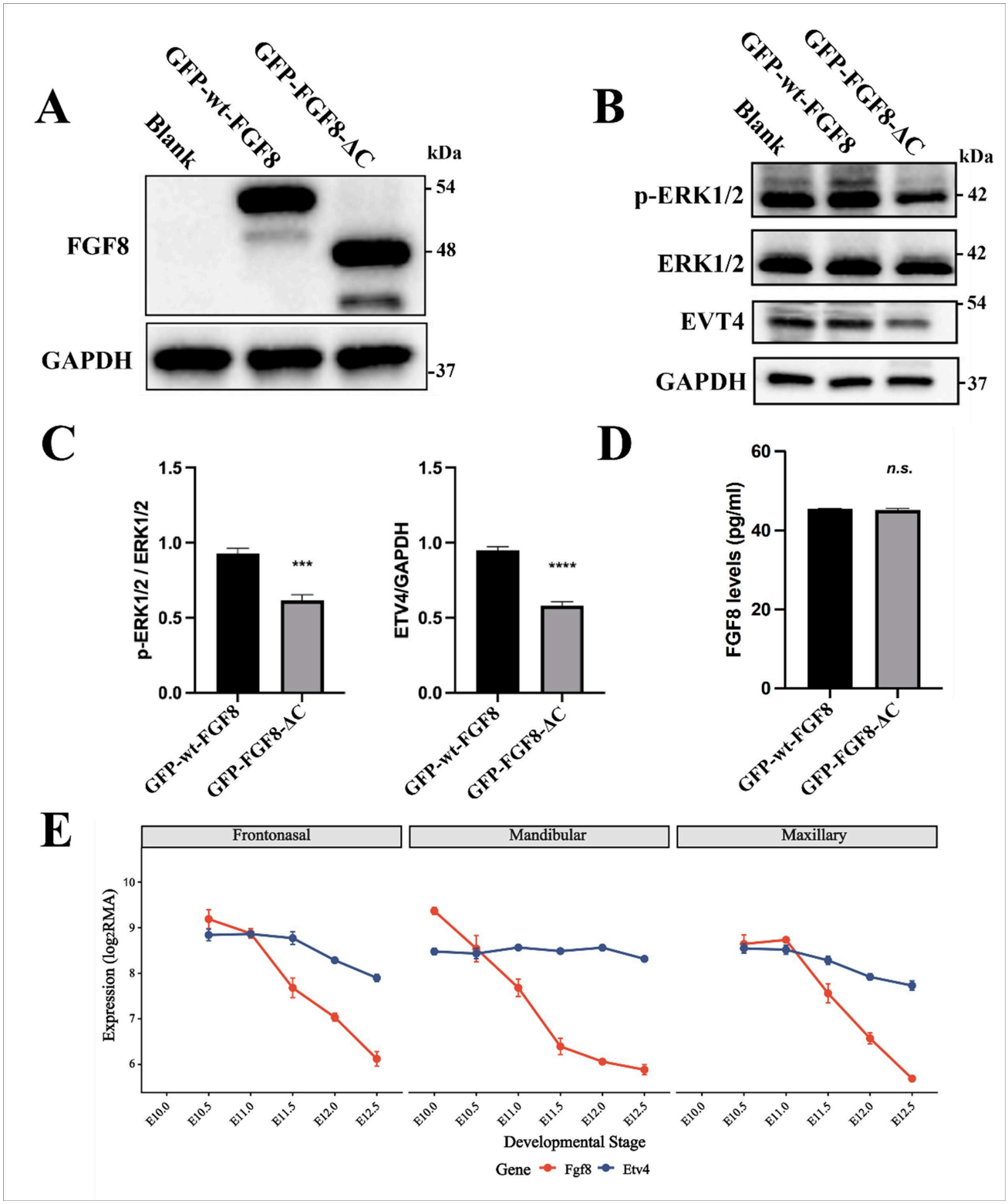


Figure 2

FGF8-ΔC impairs ERK–ETV4 signaling in HEK-293T cells.

AWestern blot analysis of GFP-tagged FGF8 protein in HEK-293T cells transfected with wild-type (WT) or mutant (MU) constructs. The mutant protein migrates at approximately 48 kDa compared to 54 kDa for wild-type, confirming production of a truncated protein. GAPDH serves as loading control. **B** Western blot analysis of phosphorylated ERK1/2 (p-ERK1/2), total ERK1/2 (t-ERK1/2), and ETV4 protein levels in WT and MU transfected cells. GAPDH serves as loading control. **C** Quantification of p-ERK1/2 (normalized to t-ERK1/2) and ETV4 (normalized to GAPDH) protein levels (n=3). **D** ELISA quantification of FGF8 protein concentration in cell culture supernatants from WT and MU transfected cells (n=3). Data are presented as mean ± SD. Statistical analysis was performed using unpaired two-tailed Student's t-test. **E**Transcriptomic expression

profiles of *Fgf8* (red) and *Etv4* (blue) in mouse embryonic frontonasal, mandibular, and maxillary prominences from E10.0 to E12.5. Data were extracted from the NCBI GEO dataset GSE7759. The y-axis represents log2 robust multi-array average (RMA) normalized expression values. The robust co-expression during this critical developmental window highlights the *in vivo* physiological relevance of the Fgf8-Etv4 signaling axis in craniofacial morphogenesis. **P<0.01, ***P<0.001, ****P<0.0001; ns, not significant.

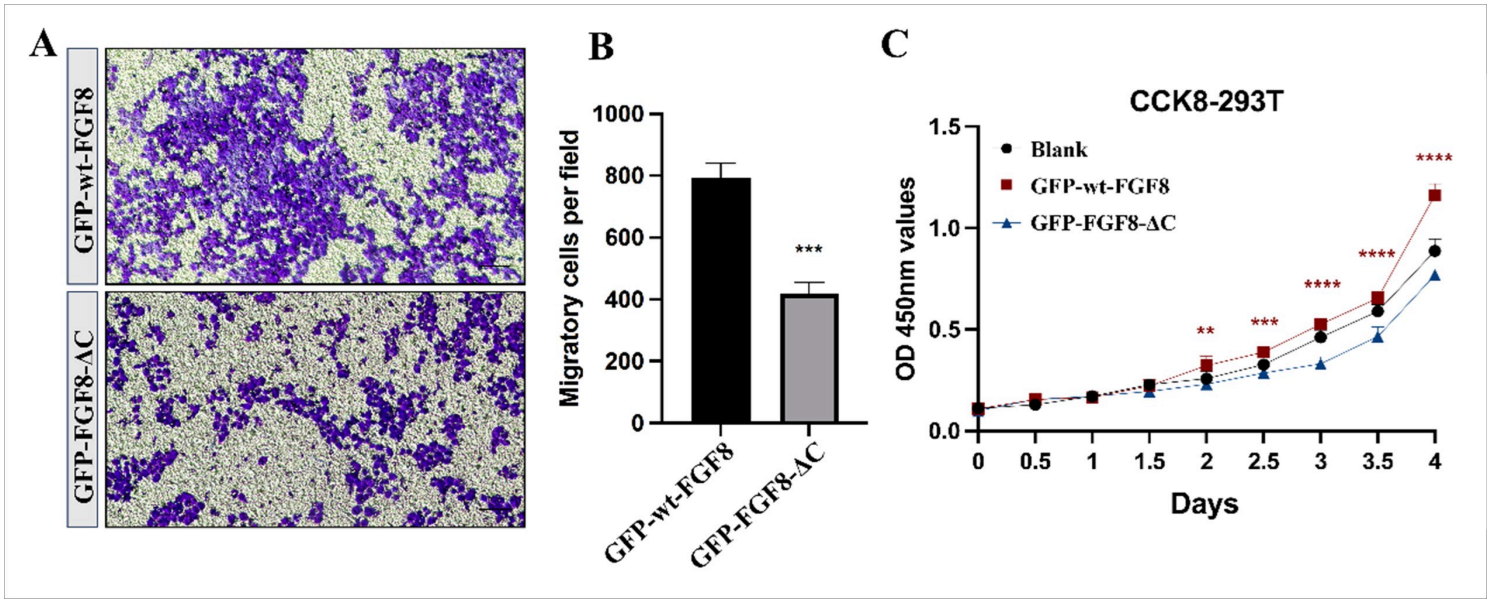


Figure 3

FGF8-ΔC inhibits migration and proliferation of HEK-293T cells.

A Representative images of Transwell migration assays showing migrated HEK-293T cells transfected with wild-type (WT) or mutant (MU) FGF8 constructs. Cells were stained with crystal violet. Scale bar, 100 μm. **B** Quantification of migrated cells per field (n=3, five fields per replicate). **C** CCK-8 cell proliferation assay measuring absorbance at 450 nm over a 4-day time course following transfection. The x-axis indicates days after cell attachment. Data are presented as mean ± SD. Statistical analysis was performed using unpaired two-tailed Student's t-test for migration assay and two-way ANOVA for proliferation assay. **P<0.01, ***P<0.001, ****P<0.0001.

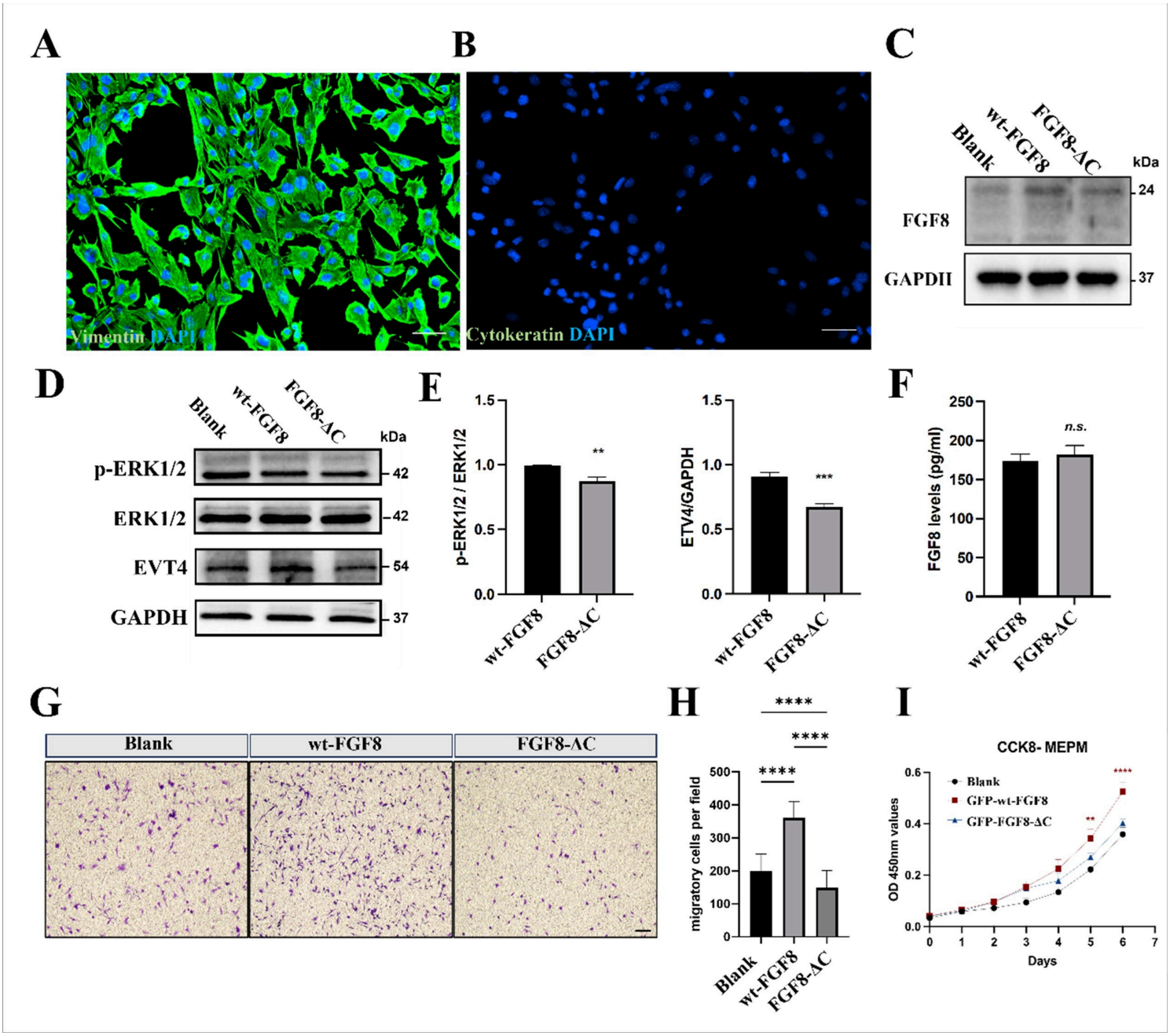


Figure 4

FGF8-ΔC impairs ERK–ETV4 signaling, migration and proliferation in primary mouse embryonic palatal mesenchymal cells.

A Immunofluorescence staining of primary MEPM cells showing positive vimentin expression (green), confirming mesenchymal cell identity. Nuclei are counterstained with DAPI (blue). Scale bar, 50 μm. **B** Immunofluorescence staining showing negative cytokeratin-19 expression, confirming absence of epithelial cell contamination. Only nuclear DAPI staining (blue) is visible. Scale bar, 50 μm. **C**Western blot analysis of FGF8 protein in WT and MU transfected MEPM cells. The mutant protein is not detected due to loss of the antibody epitope region, while a faint band in the MU lane represents endogenous FGF8. GAPDH serves as loading control. **D** Western blot analysis of p-ERK1/2, t-ERK1/2, and ETV4 protein levels in WT and MU transfected MEPM cells. **E** Quantification of p-ERK1/2 (normalized to t-ERK1/2) and ETV4 (normalized to GAPDH) protein levels (n=3). **F** ELISA quantification of FGF8 protein concentration in cell culture supernatants from WT and MU transfected MEPM cells (n=3). **G** Representative images of Transwell migration assays showing migrated MEPM cells in the Blank (untransfected control), WT Fgf8, and Fgf8-ΔC groups. Scale bar, 100 μm. **H**Quantification of migrated cells per field (n=3, five fields per replicate). The Fgf8-ΔC group shows a significant reduction in migration, falling remarkably below both the WT group and the basal level of the Blank control. I, CCK-8 cell proliferation assay over a 6-day time course. While the Fgf8-ΔC group maintains a basal growth rate slightly above the Blank control, its proliferative capacity is severely and significantly impaired compared to the WT Fgf8 group. Data are presented as mean ± SD. Statistical analysis was performed using one-way

ANOVA followed by Tukey's post hoc test for panel H, and two-way ANOVA followed by Tukey's post hoc test for panel I. **P<0.01, ***P<0.001, ****P<0.0001; ns, not significant.

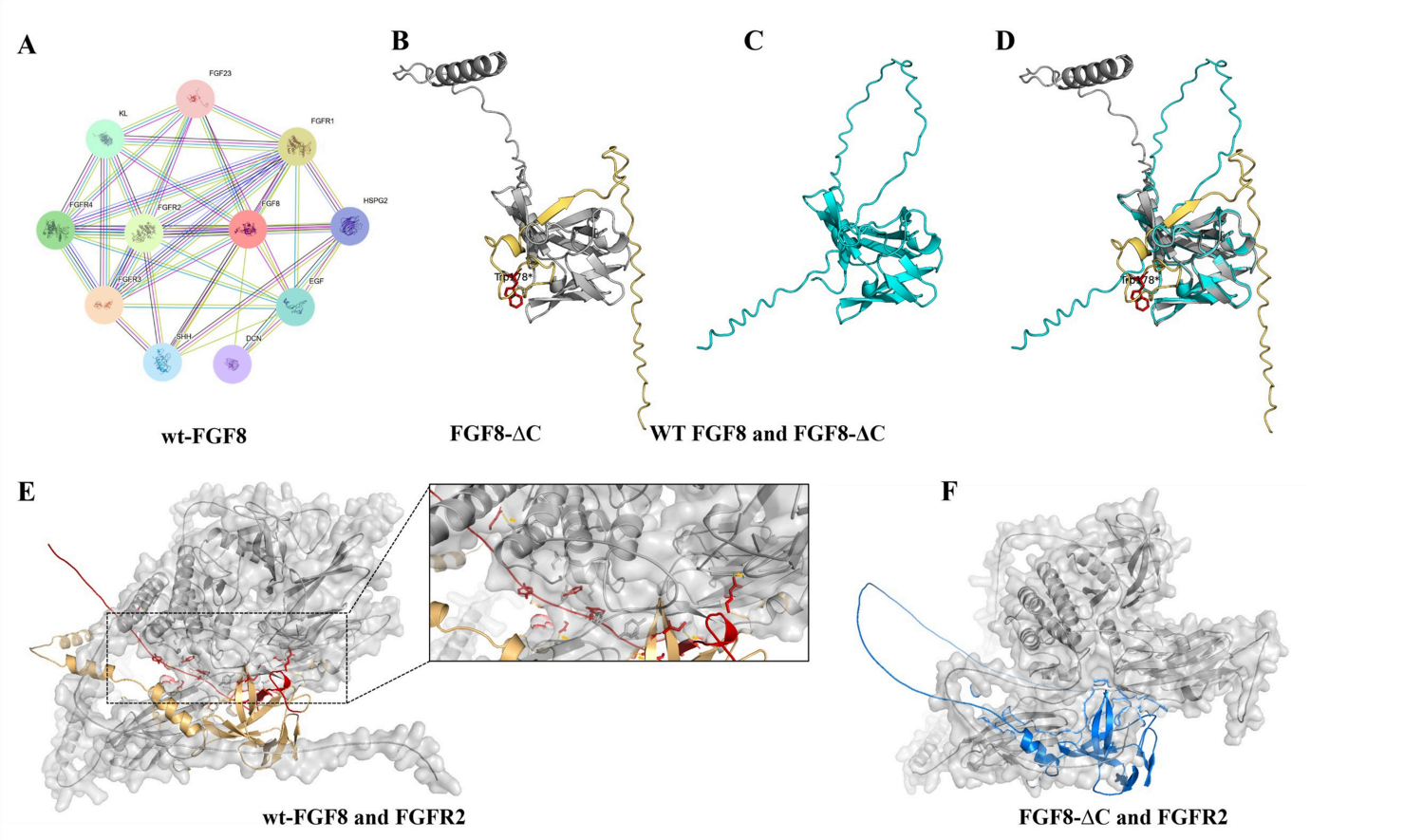


Figure 5

Structural modeling supports a plausible dominant-negative mechanism of FGF8-ΔC.

A Protein-protein interaction (PPI) network centered on FGF8 (STRING database), highlighting its primary direct interactions with fibroblast growth factor receptors (FGFR1-4) and heparan sulfate proteoglycans (e.g., HSPG2). **B** AlphaFold3-predicted monomeric structure of WT FGF8. The core β-trefoil fold is shown in grey, the C-terminal region (residues 178-244) is highlighted in yellow, and the Trp178 mutation site is depicted as red sticks. **C** Predicted structure of the truncated FGF8-ΔC mutant (cyan). **D** Superimposition of WT FGF8 and FGF8-ΔC, illustrating the complete loss of the C-terminal tail in the mutant while maintaining the core structural fold. **E** Structural model of the WT FGF8-FGFR2 complex. FGFR2 is shown as a grey surface and cartoon. The WT FGF8 core is colored in light orange, with its C-terminal tail highlighted in red. The zoom-in box details the critical binding interface, where red sticks represent interacting amino acid side chains and yellow dashed lines indicate hydrogen bonds anchoring the C-terminus to the receptor groove. **F** Structural model of the FGF8-ΔC-FGFR2 complex. The mutant ligand (blue) is capable of docking into FGFR2 (grey), but the absence of the C-terminal tail leaves a significant structural void (empty pocket) at the receptor interface, consistent with impaired receptor activation.

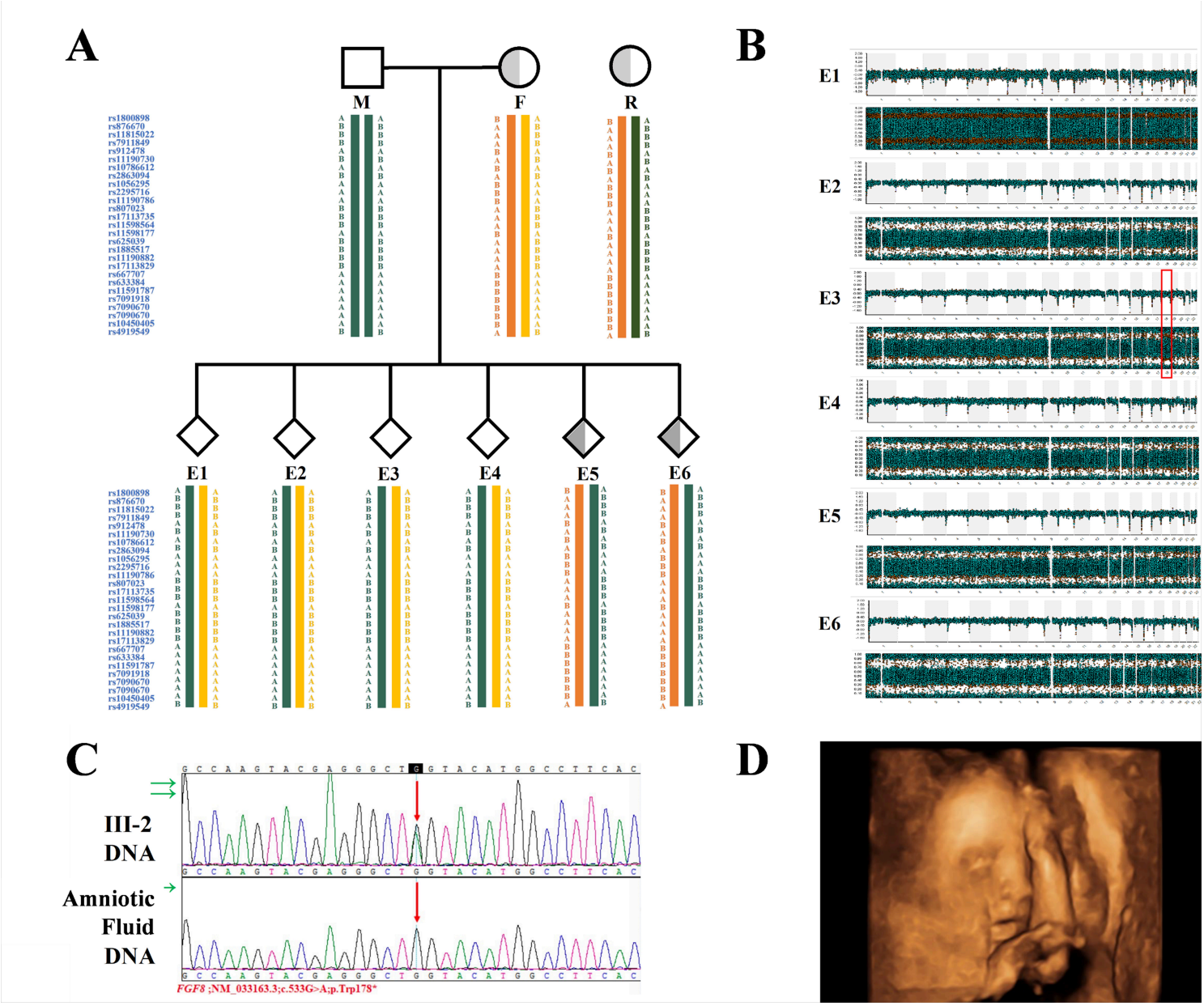


Figure 6

Preimplantation genetic testing prevented transmission of the familial FGF8 variant.

AKaryomapping haplotype analysis for determining maternal *FGF8* mutation carrier status of six embryos. The analysis was performed using SNP markers within a 2 Mb region (1 Mb upstream and 1 Mb downstream) flanking the *FGF8*locus. Blue bars represent the wild-type haplotype; red bars represent the mutant haplotype inherited from the affected mother (II-2). Embryos 1, 2, 3, and 4 inherited the wild-type maternal allele and do not carry the *FGF8*mutation; embryos 5 and 6 inherited the mutant maternal allele. **B** Copy number variation (CNV) analysis of all six embryos based on B-allele frequency and log R ratio plots. Embryo 3 shows trisomy 18 (arrow), indicated by deviation from the normal copy number pattern on chromosome 18. Embryos 1, 2, 4, 5, and 6 display normal euploid profiles. **C** Sanger sequencing chromatogram of amniotic fluid DNA obtained by amniocentesis at mid-gestation, confirming that the fetus does not carry the maternal *FGF8* c.533G>A mutation. The arrow indicates the wild-type sequence at the mutation site. **D**Prenatal ultrasound image showing normal fetal facial development without evidence of cleft lip or palate, with intact upper lip continuity and normal nasal structure.

Supplementary Files

This is a list of supplementary files associated with this preprint. Click to download.

- SupplementaryInformation.docx